Structure of the Third Intracellular Loop of the Human Cannabinoid 1 Receptor

Amy L. Ulfers,[‡] Jonathan L. McMurry,[§] Debra A. Kendall,*[,§] and Dale F. Mierke*[,‡]

Department of Molecular Pharmacology, Division of Biology and Medicine, Brown University, Providence, Rhode Island 02912, and Department of Molecular and Cell Biology, University of Connecticut, Storrs, Connecticut 06269-3044

Received April 22, 2002; Revised Manuscript Received June 27, 2002

ABSTRACT: The third cytoplasmic loop (IC3) is a determinant in the dynamic life cycle of G protein-coupled receptors, including the activation, internalization, desensitization, and resensitization processes. Here, we characterize the structural features of the IC3 of the cannabinoid 1 receptor (CB1) in micelle solution using heteronuclear, ^{1}H,^{15}N-high-resolution NMR methods. The IC3 construct was designed to contain one-third of each of the transmembrane helices (TMs 5 and 6) to tether the protein to the hydrophobic portion of the micelle. Indeed, the NMR analysis illustrates prominent α-helices at the N-terminus (G1−R10) and C-terminus (Q37−T47) of the IC3 receptor domain, corresponding to the cytoplasmic termini of TM5 and TM6. The structural features of the central portion of the IC3 consist of a small α-helix, adjacent to the terminus of TM5. The remainder is mostly unstructured as indicated by the NMR-based observables (NOEs and chemical shifts). Despite the lack of secondary structure, the hydrophobic triplet of isoleucine residues in the center of the IC3 is found in molecular dynamics simulations to associate with the lipid environment, producing two smaller loops out of the IC3. Previous studies examining mastoparan and related peptides and their ability to activate G proteins have concluded an α-helix is required for efficient binding and activation. Our structural results for the IC3 of CB1 would then suggest that in the intact receptor the G protein is activated by the α-helices of the cytoplasmic ends of TM5 or TM6 and not the unstructured central region of the IC3.

The psychoactive component of *Cannabis sativa*, Δ^9-tetrahydrocannabinol (Δ^9-THC),[1] the endogenous cannabinoids arachidonoylethanolamine (*1*), 2-arachidonylglycerol (*2*), and other cannabimimetics have a wide range of pharmacological effects, including analgesia, anti-inflammation, immunosuppression, anticonvulsion, and attenuation of vomiting (*3*). Recently, cannabinoids have also been shown to control spasticity in a multiple sclerosis mouse model system (*4*). Cannabinoids exert their effects through specific G protein-coupled receptors (GPCR)s, the CB1 and CB2 cannabinoid receptors (*5, 6*).

Cannabinoid receptors are primarily coupled to $G_{i/o}$ proteins (*7*). They impact signal transduction pathways that regulate calcium and potassium channels (*8*), adenylate cyclase, the mitogen-activated protein kinase (MAPK) pathway, and immediate early gene signaling pathways (*9*). Glass and Felder demonstrated that CB1 also couples to G_s (*10*). A mutant CB1 with a switch in the position of an alanine and leucine residue (L341A/A342L) in intracellular loop 3 (IC3) exhibited some constitutive G_s-coupled receptor activity (*11*). How and why CB1 couples to different G proteins remains a compelling question.

IC3 of CB1 has a role in receptor−G protein interactions. Synthetic peptides corresponding to the amino terminus of IC3 (residues 301−317) and the juxtamembrane carboxyl-terminal segment (residues 401−417) both autonomously inhibited adenylate cyclase (*12*). Antipeptide antibodies diminished the level of agonist-induced inhibition of adenylate cyclase without altering the binding of the agonist CP-55,940 to CB1, suggesting that the carboxyl-terminal region and IC3 are involved in G protein binding. Peptides comprising IC3 competed with the receptor for $G_{\alpha i1}$ and $G_{\alpha i2}$ binding, but not $G_{\alpha i3}$, suggesting that different G_α subtypes use different domains of the cytoplasmic loops of CB receptors for coupling (*13*). The importance of IC3 in CB1 is also underscored by the finding that S217 is a target for phosphorylation and may play a role in internalization and downregulation (*14*). Similar phenomena have been observed for peptides corresponding to soluble loops of other GPCRs (*15*−*19*).

Knowledge of GPCR structures is instrumental to developing an understanding of their functions and for generating potential therapeutic agents. Given the difficulties of crystallization of most GPCRs, including CB1, utilization of NMR for studying isolated receptor domains can be particularly insightful. We have established a procedure of examining domains of GPCRs incorporating significant portions of the TM domains which serve to tether the receptor construct to

* To whom correspondence should be addressed. D.F.M.: Department of Molecular Pharmacology, Division of Biology and Medicine, Brown University, Providence, RI 02912; phone, (401) 863-2139; fax, (401) 863-1595; e-mail, Dale_Mierke@Brown.edu. D.A.K.: Department of Molecular and Cell Biology, University of Connecticut, Storrs, CT 06269-3044; phone, (860) 486-1891; fax, (860) 486-1784; e-mail, Debra.A.Kendall@Uconn.edu.

‡ Brown University.

§ University of Connecticut.

[1] Abbreviations: CB1, brain cannabinoid receptor; CB2, peripheral cannabinoid receptor; Δ^9-THC, Δ^9-tetrahydrocannabinol; GPCR, G protein-coupled receptor; SDS, sodium dodecyl sulfate; GST, glutathione *S*-transferase; IC, intracellular loop; NMR, nuclear magnetic resonance; DG, distance geometry; MD, molecular dynamics.

10.1021/bi0259610 CCC: $22.00
Published on Web 08/24/2002

the lipid environment and facilitate the incorporation of the structural data into receptor models based on the TM topology of rhodopsin (*20*−*22*). Yeagle, Albert, and co-workers have carried out studies on rhodopsin itself using organic solvents (*23*). They found that the peptide containing the sequence of IC3 inhibited light-stimulated activation of rhodopsin, providing additional evidence that the synthetic peptide, apart from the receptor, adopted a biologically active conformation. This procedure has been applied to other parts of rhodopsin and more recently to bacteriorhodopsin (*24*−*27*). Other studies include examination of the angiotensin 1 (*28*, *29*) and adrenergic receptors (*30*).

A molecular model of CB1 has been proposed (*31*), but detailed structural information is still lacking, particularly for the extracellular and cytoplasmic portions of the receptor. Here, we describe the structural characterization of IC3 of CB1. The sequence of the entire loop was expressed as a GST fusion in *Escherichia coli*, labeled with ^{15}N, purified, and cleaved to yield the isolated IC3 domain of CB1. The structure of the loop was then determined by high-resolution NMR. We chose to begin with the IC3 loop given its demonstrated importance in G protein interactions, thus playing an important role in the life cycle of the receptor.

MATERIALS AND METHODS

Materials. The sequence of the third intracellular loop of CB1 was amplified according to standard protocols from plasmid pCNCB1 (*32*) using site-specific oligonucleotides containing *Bam*HI and *Eco*RI restriction sites through which the product was cloned into plasmid pGEX-2T (Amersham BioSciences, Piscataway, NJ). The resulting plasmid, pGEX2T.CB1IC3, encoded a fusion of glutathione *S*-transferase (GST) N-terminal to the IC3 peptide. This construct included a linker region between the GST and the peptide, which encodes a thrombin recognition site, LVPRGS. After thrombin cleavage, a peptide of the sequence GSK-AHSHAVRMIQRGTQKSIIIHTSEDGKVQVTRPDQAR-MDIRLAKT is generated. The amino-terminal residues, Gly and Ser, correspond to part of the GST linker region, and the remainder corresponds to IC3 of CB1.

Expression and Purification of IC3. Plasmid pGEX2T. CB1IC3 was transformed into *E. coli* strain BL21(DE3) (Invitrogen, Carlsbad, CA). A culture of M9 medium (*33*) with 250 μg/mL ampicillin was inoculated with a single colony, grown at 37 °C overnight, and then subcultured 1:100 into 12 L of M9 containing $^{15}NH_4Cl$ and 250 μg/mL ampicillin. Cells were grown at 37 °C until the OD_{600} reached 0.5, induced with 0.1 mM IPTG for 4 h, and harvested by centrifugation at 8000*g* for 15 min. Cells were resuspended in 1× PBS [140 mM NaCl, 2.7 mM KCl, 10 mM Na_2HPO_4, 1.8 mM KH_2PO_4 (pH 7.3), and 0.1 mM PMSF] and sonicated on ice for 3 min. Triton X-100 was then added to 1% (v/v), and the crude lysate was stirred at 4 °C for 30 min. The lysate was then centrifuged for 30 min at 22500*g*. The supernatant was mixed in batch with 1.25 mL/L of original culture of glutathione Sepharose 4B (Amersham Bio-Sciences), previously equilibrated in 1× PBS, and stirred at 4 °C for 1 h. The suspension was then loaded onto a 0.7 cm × 20 cm column and allowed to flow through by gravity. The resin was washed with 10 bed volumes of ATP wash [50 mM Tris (pH 7.0), 50 mM KCl, 20 mM $MgCl_2$, and 5 mM ATP] to remove a contaminating ∼70 kDa protein that behaved like DnaK (*34*). Additional washes of 2 × 10 bed volumes of 1× PBS were carried out. The fusion protein was eluted by gravity with 1 bed volume of 50 mM Tris (pH 8.0), 5% glycerol, 10 mM reduced glutathione, and 1% (w/v) CHAPS. Repeated elution with 1 bed volume was done until all significant quantities of the protein had eluted as determined by a Bradford assay. All fractions were then combined, and the GST was cleaved from the peptide overnight at 22 °C with 100 units of thrombin. Cleavage reaction products were chilled to 4 °C and spun at 5900*g* for 15 min to remove precipitants. The supernatant was diluted 10-fold in dH_2O and loaded onto a 2 mL SP-Sepharose Fast Flow column at a flow rate of 1.25 mL/min. The column was washed with 30 bed volumes of 0.1× PBS followed by 5 bed volumes of 10 mM ammonium acetate. Peptide was then eluted with a continuous 100 mL linear gradient of ammonium acetate from 0 to 500 mM flowing at a rate of 0.5 mL/min. Fractions of 1.5 mL were collected and analyzed by SDS−PAGE with silver staining to visualize the peptides. Pure peptide-containing fractions were combined and lyophilized. The lyophilized material was dissolved into 5% acetic acid and lyophilized again. Dissolution was repeated twice more to ensure that the ammonium acetate had been removed into the vapor phase. Approximately 42 mg of peptide was obtained from the 12 L of M9 culture.

NMR Measurements. All spectra were acquired on a 600 MHz AVANCE spectrometer at 310 K. The IC3 receptor domain was dissolved in 200 mM sodium dodecyl sulfate micelles (Cambridge Isotope Laboratories, Inc., Andover, MA) in 50 mM phosphate buffer (pH 6.5). Deuterium oxide (10%) was used as a lock signal, and 1 mM 3-(trimethylsilyl)tetradeuteriosodium propionate (TSP) was added as an internal chemical shift reference.

Spectral Assignment. Two-dimensional (2D) NOESY, TOCSY, and ^{1}H−^{15}N HSQC and three-dimensional (3D) ^{1}H−^{15}N NOESY-HSQC and ^{1}H−^{15}N TOCSY-HSQC spectra were acquired. The NOESY type experiments were collected with mixing times ranging between 80 and 160 ms, while both DIPSI and MLEV pulse trains were implemented for TOCSY experiments, typically for 45 ms. The WATERGATE sequence was used for suppression of the water signal. Spectra were processed using Bruker XWIN NMR software or NMRPipe (*35*). Partial sequential assignments were made using 2D TOCSY (*36*, *37*) and NOESY (*38*) spectra; overlapped residues were resolved using the 3D HSQC-TOCSY and HSQC-NOESY spectra. Sparky (*39*) was used to view and assign spectra, and to measure peak volumes and intensities.

Distance Geometry Calculations. Peak intensities from the assigned NOESY spectra were divided into strong, medium, and weak peaks to generate distance restraints (2.0−3.0, 2.0−4.0, and 2.0−5.0 Å, respectively) for preliminary structure calculations. Pseudoatoms were used for methylene protons that could not be stereospecifically assigned and the upper distances corrected according to the method proposed by Wüthrich and co-workers (*40*). Distance geometry calculations were carried out using a home-written program employing the random metrization method of Havel (*41*) to generate an ensemble of structures consistent with observed distance restraints.

Modeling and Molecular Dynamics. Distance geometry structures were energy-minimized using the Discover program within the Insight II package (Molecular Simulations, Inc., San Diego, CA). The transmembrane helices of the IC3 receptor domain were template forced to the corresponding regions, TM5 and TM6, of rhodopsin, using the X-ray structure of rhodopsin (*42*). During this energy minimization, the helical regions, indicated by the secondary shift of the chemical shifts, had a small forcing potential (200 kcal/mol) applied to the ϕ and ψ dihedral angles with target values of $-57.0°$ for ϕ and $-47.0°$ for ψ. The resulting structures were then subjected to 300 ps of molecular dynamics within a two-phase box of water and decane using GROMACS. Typically, the boxes had a volume of 310 nm^3 containing approximately 340 molecules of decane and 4200 molecules of water. Atoms of the peptide and water were treated explicitly. The CH_2 and CH_3 groups of decane were treated as united atoms, using the Ryckaert−Bellemans potential. The velocities were recalculated every 2 fs; neighbors lists for long-range interactions were updated every 20 fs, and the resulting trajectories were sampled every 0.5 ps.

RESULTS AND DISCUSSION

As expected for a hydrophobic receptor domain, IC3 of CB1 produced by thrombin cleavage of the GST fusion protein was prone to extensive aggregation at the concentrations required for NMR-based structural studies. Use of Triton X-100, CHAPS, and glycerol mitigated the problem during the protein purification steps. For the NMR experiments, the solubility of IC3 was evaluated in dodecylphosphocholine (DPC) and sodium dodecyl sulfate (SDS), two systems well characterized for the study of peptides, hormones, and receptor domains (*43*−*45*). The IC3 construct was not sufficiently soluble in DPC, and therefore, micelles of SDS were used for the studies described here. Upon comparison of the one-dimensional (1D) ^{1}H spectra of CB1 IC3 in aqueous solution, the receptor domain appears to adopt a conformation in the presence of the micelles, consistent with previous observations that peptides adopt stable conformations when associated with micelles (*46*, *47*). The increase in the ^{1}H line widths is consistent with the association of the IC3 domain with the micelle.

In the homonuclear 2D TOCSY and NOESY spectra of the ^{15}N-labeled IC3 receptor domain, most of the cross-peaks in the Hα−HN region were overlapped (see Figure 1). Therefore, the use of Hα−HN(i + 1) peaks provided only a partial assignment. To obtain a complete assignment, 3D HSQC-TOCSY and HSQC-NOESY spectra were acquired. These spectra resolved the overlapping resonances, allowing for the unambiguous assignment of 44 of the 47 residues. The Hα−Hα peak of the N-terminal glycine residue is not clearly distinguishable from the diagonal, and the Hα and side chain protons of the C-terminal threonine are not visible. In addition, the Hδ side chain peaks of P33 cannot be unambiguously assigned, although the sequential Hα−HN(i + 1) is clearly visible. The assignment of the 3D spectra also allows the complete assignment of the 2D NOESY spectrum with the help of the HSQC spectrum, although overlap prevents accurate integration of some of the peaks.

In Figure 2, the secondary shift analysis (using a running average of three residues) of the Hα resonances (*48*) of the IC3 receptor domain of CB1 is illustrated. The secondary shifts provide valuable confirmatory structural information, particularly when many NOE volumes cannot be determined because of spectral overlap. Previously, in cases where the resolution of NOEs is not problematic, we and others have shown a good correlation with the secondary shift analysis and NOEs in the presence of micelles (*22*, *49*−*51*). The N-terminus of the peptide, stretching from S2 to R10, shows consistently negative chemical shifts in comparison to the values for a random coil, consistent with the presence of an α-helix. The secondary shift analysis also shows a less defined helix between residues I12 and S19, indicated by consistently negative chemical shifts of less than 0.1 ppm. Positive values from I21 to D27 and from K29 to Q31 are broken by neutral or slightly negative shifts around residue G28, which may be consistent with a turn in the peptide (*48*). Finally, the C-terminus, between residues V32 and K46,

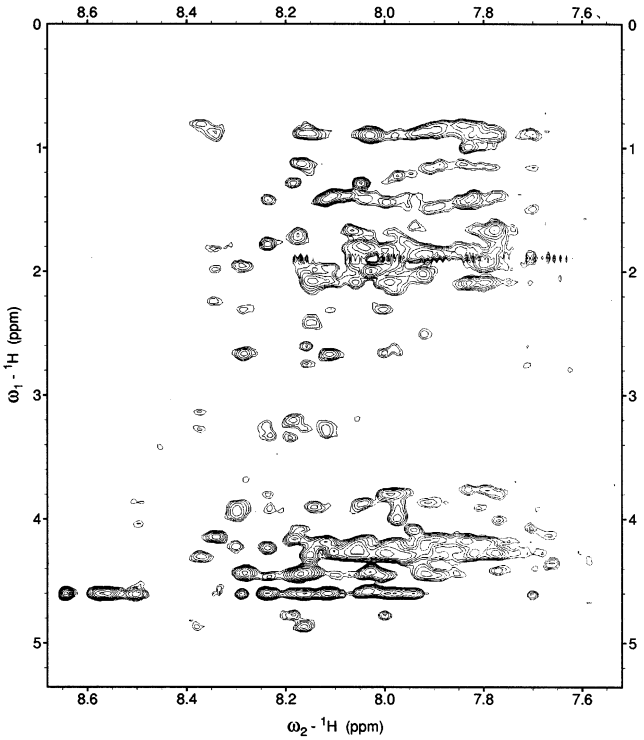

FIGURE 1: Expanded portion of a two-dimensional NOESY spectrum of the IC3 domain of CB1, CB1(300−343), recorded at 310 K with a mixing time of 150 ms.

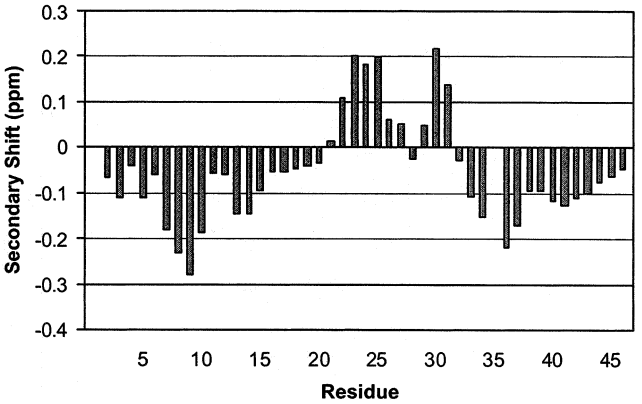

FIGURE 2: Hα secondary shifts of the IC3 domain of CB1, CB1-(300−343). The chemical shifts were measured relative to TSP at 310 K.

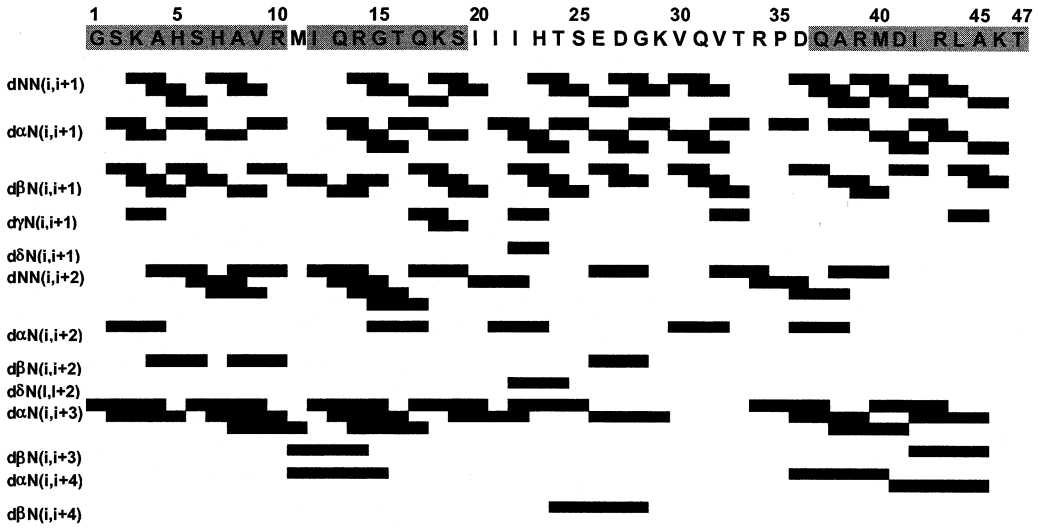

FIGURE 3: Summary of structurally informative NOEs calculated from $^1H-^1H$ NOESY and $^1H-^{15}N$ HSQC-NOESY spectra of the IC3 domain of CB1.

is consistently negatively shifted, defining the beginning of TM6 of the CB1 receptor.

The distance restraints were generated from the assigned 2D NOESY and 3D NOESY-HSQC spectra. The severe overlap of the signals prohibited integration of the cross-peak volumes; therefore, the NOEs were classified as strong, medium, and weak estimated from the 2D and 3D spectra, resulting in a set of 308 distance restraints. The structurally relevant NOEs are shown schematically in Figure 3. The NOEs defining the secondary structural elements are described below.

Helix I is made up of residues G1−R10. The NOEs include Hα(*i*)−NH(*i* + 3) cross-peaks for *i* values of 1, 2, 6, 7, and 8, NH(*i*)−NH(*i* + 1) peaks for 3, 4, 5, 7, and 8, and NH(*i*)−NH(*i* + 2) peaks for 4, 6, 7, and 8. All of these NOEs are consistent with the significant negative chemical shift in this region, indicating a well-defined α-helix.

Helix II is made up of residues I12−S19. The NOEs describing this α-helix include Hα(*i*)−NH(*i* + 3) cross-peaks for *i* values of 12, 13, 14, 17, and 19, NH(*i*)−NH(*i* + 1) peaks for *i* values of 14, 15, 17, 18, and 19, NH(*i*)−NH(*i* + 2) peaks with *i* values of 12, 13, 14, 15, and 17, and an Hα(*i*)−NH(*i* + 4) cross-peak for an *i* value of 11.

Helix III is made up of residues Q37−T47. The NOEs include Hα(*i*)−NH(*i* + 3) peaks for *i* values of 36, 38, 40, and 42, Hα(*i*)−NH(*i* + 4) peaks for *i* values of 36 and 41, NH(*i*)−NH(*i* + 1) peaks for *i* values of 36, 37, 38, 39, 40, 41, 42, 43, and 45, and NH(*i*)−NH(*i* + 2) peaks for *i* values of 36 and 38.

The resulting structures from the metric matrix DG calculations contained the three α-helices, consistent with the NOE-derived distance restraints. The three domains are relatively well defined, with rmsd values of 2.0, 1.7, and 1.4 Å, for the backbone atoms for residues 1−10, 12−19, and 37−47, respectively. The topological arrangement of the three helices is not defined, as illustrated by an rmsd value of 8.7 Å for all backbone atoms. In Figure 4, the dihedral angle order parameters, as described by Havel (*52*), of the resulting DG structures are given. The high values, close to 1.0, for the three helices illustrate convergence of the secondary structural elements. We find that although the metric matrix DG calculations provide superior conformational searching, α-helices are sometimes removed from standard values (e.g., ϕ values ranged from −30 to −85° in the resulting DG structures). This can be attributed to ignoring hydrogen bonds as well as a problem with the determination of the correct handedness of the α-helices based solely on distances. More standard α-helices, consistent with the secondary shift values, were introduced into the structures during energy minimization (100 steps of steepest descent) with application of a dihedral angle constraints for the three α-helices, within residues G1−R10, I12−S19, and Q37−T47.

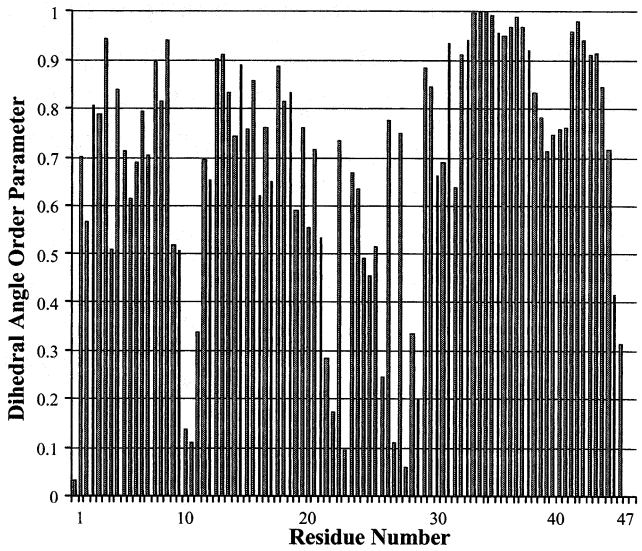

FIGURE 4: Dihedral angle order parameters calculated for the resulting DG structures of the IC3 domain of CB1. The order parameters (*52*) range from values of 1.0, indicating perfect convergence, to 0.0, indicating a complete lack of structural convergence.

No NOEs were observed between the transmembrane helices in the IC3 domain of CB1 to provide information about the relative orientation within the micelle. The lack of NOEs is not surprising based on the X-ray structure of rhodopsin (the closest approach of protons on different TM helices is 8−10 Å) (*42*). Therefore, the crystal structure of bovine rhodopsin was used as a template for the transmembrane regions of the IC3 domain of CB1. To incorporate

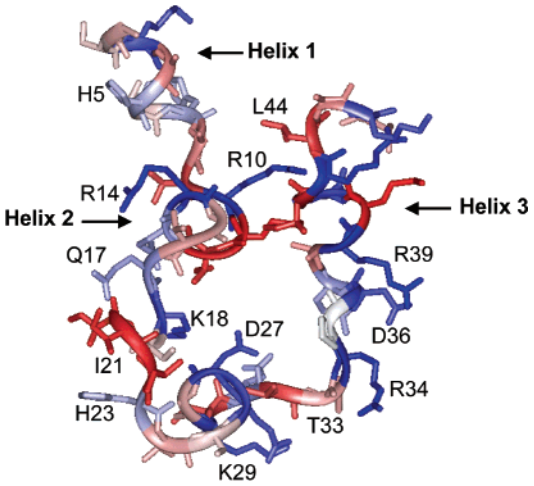

FIGURE 5: Structure of the IC3 domain of CB1, CB1(300−343), following NOE-restrained MD simulations for 300 ps in a water/decane membrane mimetic solvent box with periodic boundary conditions. The amino acids of the receptor fragment are color-coded according to hydrophobicity (blue for polar and red for hydrophobic). Many of the residues and the three α-helices are denoted.

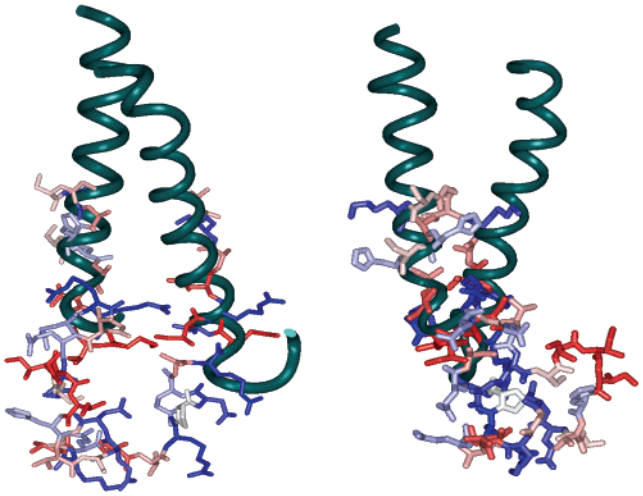

FIGURE 6: Two views (90° rotation) of the structure of the IC3 domain of CB1 after 300 ps of MD simulation, superimposed on TM5 and TM6 of the crystal structure of bovine rhodopsin (green). The amino acids of the receptor are colored blue for polar residues and red for hydrophobic residues.

the observed structural features of IC3 of CB1 into the model of the GPCR, the N- and C-terminal helices were template forced to the corresponding regions of TM5 and TM6 of rhodopsin (*42*). The sequence alignment of IC3 of CB1 with rhodopsin is shown below (with the TM helices observed for CB1 denoted in bold).

CB1:

```
300          310          320          330          340  343
  KAHSHAVRMIQRGTQKSIIIHTSEDGKVQVTRPDQARMDIRLAKT
```

Bovine Rhod.

```
  FCYGQLVFTVK-----------EAAAQQQESATTQKAEKEVTRM
221          231          232                  253
```

This model, accounting for all of the experimental NMR data and in accord with the topological arrangement of the TM helices of rhodopsin, was then subjected to extensive MD simulations. The water/decane box used for the MD simulations reproduces the biphase character of the aqueous micelle solution. The decane molecules mimic the hydrophobic phase created by the alkylic chains of the SDS molecules (*22*). In this simulation system, the correct description of the charge interface, created by the phosphate and choline groups of the DPC, is sacrificed for simplicity and computational speed, which in turn allows for extended simulations and examination of multiple starting structures. The goal of the simulations is further refinement and verification of the energetic stability of the DG-generated structures in an environment similar to that used for the NMR experiments. The N- and C-terminal helices, corresponding to the cytoplasmic termini of TM5 and TM6, were placed into the decane layer, and the simulation was carried out for 300 ps. A representative final structure after the MD simulation is shown in Figure 5. Removal of the NOEs and extending the simulation for an additional 500 ps produced no significant conformational changes.

During the NOE-restrained MD simulation, the overall structural features and topology with respect to the hydrophobic and hydrophilic phases are maintained. The N- and C-termini, corresponding to the TM helices, restrained only by the NOEs, are quite stable and remain within the decane layer. The orientation between the helices, with small variations, is maintained during the simulation; superimposing the final structure with the TM helices of rhodopsin illustrates only minor changes (root-mean-square deviations of 1.8 Å for K3−R10 and 1.6 Å for R29−K46). The structure of the peptide after 300 ps of MD simulation is shown superimposed on TM5 and TM6 of the rhodopsin crystal structure in Figure 6. There is no significant interaction between the TM helices; in the final structure, the shortest Cα−Cα distance between the TM helices is more than 8 Å. Interestingly, both the N- and C-terminal helices in the CB1 receptor domain examined here are not extremely hydrophobic in nature and yet are found to be stable in the hydrophobic phase during the simulations.

The central portion of the IC3 domain is also found to be closely associated with the hydrophobic phase during the structure refinement. The α-helix consisting of residues I12−S19 is amphipathic, and the hydrophobic face of the helix projects toward the decane phase. Additionally, the triad of isoleucine residues at the end of this helix acts to anchor this portion of the IC3 loop to the hydrophobic phase. The sequence between residues I20 and Q37 does not show any defined secondary structure, and moves through the water layer of the simulation cell during the molecular dynamics simulation. This portion of the IC3 receptor domain of CB1 exhibits the most flexibility and dynamics during the simulations.

Studies targeting the IC3 domain of GPCRs have shown that both the N- and C-termini of the cytoplasmic loop play important roles in G protein coupling, being partially responsible for the G protein specificity of the receptor (*53*−*57*). Structural studies, including this one, have indicated that these regions are α-helical (*20*, *21*, *30*). Indeed, the activation of G proteins by mastoparan has been proposed to function through mimicking the α-helix of the IC3 loop (*58*−*60*). In bovine rhodopsin, a periodic series of residues (226, 229, 230, 233, and 234) in the N-terminal region of the solvent-

exposed IC3 loop has been shown by cysteine substitution mutagenesis to be critical for activation of transducin (*61*). On the basis of incorporation of spin-labels, these residues have been shown to be on the solvent-exposed face of a helix and undergo greater motion than the rest of the loop (*62*). It is interesting to note that this helix corresponds to the helix observed in residues I12−S19 of the CB1 receptor.

In the structure presented here, the C-terminus of the IC3 loop forms an α-helix, entering the membrane at Q37 (corresponding to Q334 of CB1). This places the L341 and A342 residues, which have been shown to alter G protein coupling of CB1 (*11*), approximately one helical turn up in TM6. There are two possible explanations for how this might occur. First, this portion of the TM helix may be oriented along the membrane surface, with the hydrophobic face of the helix projecting toward the membrane and the hydrophilic face out toward the solvent. This orientation may be a result of a bend in TM6, similar to the bend observed in the crystal structure of TM6 of bovine rhodopsin at P267 (*42*). CB1 has an analogous proline (P358), which makes it likely that TM6 is also bent in this receptor. A second possibility is that the TM6 helix extends somewhat out of the membrane on the cytoplasmic side. In the crystal structure of rhodopsin, TM6 extends out of the membrane by approximately four residues on the cytoplasmic side (*42*). Additionally, recent investigations using the incorporation of fluorescent probes at this region of the β-adrenergic receptor have shown significant movement, particularly with respect to orientation relative to the membrane surface (*63*, *64*). This conformational change may expose part of the receptor that is necessary for binding and activation of the Giα; more specifically, hydrophobic residues in this region may become available to interact with the Gα subunit.

Although the IC3 loop of rhodopsin is shorter than that of CB1, the sequence homology may suggest a common mechanism for G protein coupling. In the X-ray structure of rhodopsin, the IC3 loop is highly flexible; indeed, several residues (Q236−E239) could not be resolved in the crystal. There are no defined regions of secondary structure in the loop, and it appears to lie across the membrane rather than making contact with other regions of the cytoplasmic face of the receptor. This is in good agreement with our result of a flexible loop that interacts readily with the membrane.

In conclusion, we have determined the structure of the third intracellular loop of the CB1 receptor and examined it in the context of a receptor using the topological orientation of the TM helices of rhodopsin. The central portion of IC3 is found to be mostly unstructured, with well-defined helices forming the cytoplasmic ends of TM5 and TM6. Interestingly, most of the residues identified as being important for activation of the G-protein are located at the beginning of TM6, supporting a translation of the helix into the cytoplasmic space upon receptor activation.

REFERENCES

1. Devane, W. A., Hanus, L., Breuer, A., Pertwee, R. G., Stevenson, L. A., Griffin, G., Gibson, D., Mandelbaum, A., Etinger, A., and Mechoulam, R. (1992) *Science 258*, 1946−1949.
2. Mechoulam, R., Ben-Shabat, S., Hanus, L., Ligumsky, M., Kaminski, N. E., Schatz, A. R., Gopher, A., Almog, S., Martin, B. R., Compton, D. R., et al. (1995) *Biochem. Pharmacol. 50*, 83−90.
3. Dewey, W. L. (1986) *Pharmacol. Rev. 38*, 151−178.
4. Baker, D., Pryce, G., Croxford, J. L., Brown, P., Pertwee, R. G., Huffman, J. W., and Layward, L. (2000) *Nature 404*, 84−87.
5. Matsuda, L. A., Lolait, S. J., Brownstein, M. J., Young, A. C., and Bonner, T. I. (1990) *Nature 346*, 561−564.
6. Munro, S., Thomas, K. L., and Abu-Shaar, M. (1993) *Nature 365*, 61−65.
7. Howlett, A. C., Qualy, J. M., and Khachatrian, L. L. (1986) *Mol. Pharmacol. 29*, 307−313.
8. Howlett, A. C. (1995) in *Cannabinoid Receptors*: *Molecular Biology & Pharmacology* (Pertwee, R. G., Ed.) pp 167−204, Academic Press, London.
9. Bouaboula, M., Poinot-Chazel, C., Bourrie, B., Canat, X., Calandra, B., Rinaldi-Carmona, M., Le Fur, G., and Casellas, P. (1995) *Biochem. J. 312*, 637−641.
10. Glass, M., and Felder, C. C. (1997) *J. Neurosci. 17*, 5327−5333.
11. Abadji, V., Lucas-Lenard, J. M., Chin, C., and Kendall, D. A. (1999) *J. Neurochem. 72*, 2032−2038.
12. Howlett, A. C., Song, C., Berglund, B. A., Wilken, G. H., and Pigg, J. J. (1998) *Mol. Pharmacol. 53*, 504−510.
13. Mukhopadhyay, S., and Howlett, A. C. (2001) *Eur. J. Biochem. 268*, 499−505.
14. Garcia, D. E., Brown, S., Hille, B., and Mackie, K. (1998) *J. Neurosci. 18*, 2834−2841.
15. Varrault, A., Le Nguyen, D., McClue, S., Harris, B., Jouin, P., and Bockaert, J. (1994) *J. Biol. Chem. 269*, 16720−16725.
16. Lechleiter, J., Hellmiss, R., Duerson, K., Ennulat, D., David, N., Clapham, D., and Peralta, E. (1990) *EMBO J. 9*, 4381−4390.
17. Lee, N. H., Geoghagen, N. S., Cheng, E., Cline, R. T., and Fraser, C. M. (1996) *Mol. Pharmacol. 50*, 140−148.
18. Wade, S. M., Scribner, M. K., Dalman, H. M., Taylor, J. M., and Neubig, R. R. (1996) *Mol. Pharmacol. 50*, 351−358.
19. Wade, S. M., Dalman, H. M., Yang, S. Z., and Neubig, R. R. (1994) *Mol. Pharmacol. 45*, 1191−1197.
20. Mierke, D. F., Royo, M., Pellegrini, M., Sun, H., and Chorev, M. (1996) *J. Am. Chem. Soc. 118*, 8998−9004.
21. Pellegrini, M., Royo, M., Chorev, M., and Mierke, D. F. (1996) *J. Pept. Sci. 40*, 653−666.
22. Pellegrini, M., Bisello, A., Rosenblatt, M., Chorev, M., and Mierke, D. F. (1998) *Biochemistry 37*, 12737−12743.
23. Yeagle, P. L., Alderfer, J. L., and Albert, A. D. (1995) *Biochemistry 34*, 14621−14625.
24. Yeagle, P. L., Alderfer, J. L., and Albert, A. D. (1997) *Biochemistry 36*, 9649−9654.
25. Yeagle, P. L., Choi, G., and Albert, A. D. (2001) *Biochemistry 40*, 11932−11937.
26. Katragadda, M., Alderfer, J. L., and Yeagle, P. L. (2001) *Biophys. J. 81*, 1029−1036.
27. Katragadda, M., Chopra, A., Bennett, M., Alderfer, J. L., Yeagle, P. L., and Albert, A. D. (2001) *J. Pept. Res. 58*, 79−89.
28. Franzoni, L., Nicastro, G., Pertinhez, T. A., Tato, M., Nakaie, C. R., Paiva, A. C. M., Schreier, S., and Spisni, A. (1997) *J. Biol. Chem. 272*, 9734−9741.
29. Franzoni, L., Nicastro, G., Pertinhez, T. A., Oliveira, E., Nakaie, C. R., Paiva, A. C., Schreier, S., and Spisni, A. (1999) *J. Biol. Chem. 274*, 227−235.
30. Chung, D. A., Zuiderweg, E. R., Fowler, C. B., Soyer, O. S., Mosberg, H. I., and Neubig, R. R. (2002) *Biochemistry 41*, 3596−3604.
31. Bramblett, R. D., Panu, A. M., Ballesteros, J. A., and Reggio, P. H. (1995) *Life Sci. 56*, 1971−1982.
32. Chin, C. N., Lucas-Lenard, J., Abadji, V., and Kendall, D. A. (1998) *J. Neurochem. 70*, 366−373.
33. Sambrook, J., Fritsch, E. F., and Manitatis, T. (1989) *Molecular Cloning*: *A Laboratory Manual*, 2nd ed., Cold Spring Harbor Laboratory Press, Plainview, NY.
34. Sherman, M., and Goldberg, A. L. (1992) *EMBO J. 11*, 71−77.
35. Delaglio, F., Grzesiek, S., Vuister, G. W., Zhu, G., Pfeifer, J., and Bax, A. (1995) *J. Biomol. NMR 6*, 277−293.
36. Braunschweiler, L., and Ernst, R. R. (1983) *J. Magn. Reson. 53*, 521−528.
37. Bax, A., and Davis, D. G. (1985) *J. Magn. Reson. 65*, 355−360.
38. Macura, S., Huang, Y., Suter, D., and Ernst, R. R. (1981) *J. Magn. Reson. 43*, 259−281.
39. Goddard, T. D., and Kneller, D. G. (2001) *Sparky*, University of California, San Francisco.
40. Wuthrich, K., Billeter, M., and Braun, W. (1983) *J. Mol. Biol. 169*, 949−961.
41. Havel, T. F. (1991) *Prog. Biophys. Mol. Biol. 56*, 43−78.

42. Palczewski, K., Kumasaka, T., Hori, T., Behnke, C. A., Motoshima, H., Fox, B. A., Le Trong, I., Teller, D. C., Okada, T., Stenkamp, R. E., Yamamoto, M., and Miyano, M. (2000) *Science 289*, 739−745.
43. Bairaktari, E., Mierke, D. F., Mammi, S., and Peggion, E. (1990) *Biochemistry 29*, 10090−10096.
44. Kallick, D. A., Tessmer, M. R., Watts, C. R., and Li, C. (1995) *J. Magn. Reson., Ser. B 109*, 60−65.
45. Liu, L. P., and Deber, C. M. (1997) *Biochemistry 36*, 5476−5482.
46. Bosch, C., Brown, L. R., and Wuthrich, K. (1980) *Biochim. Biophys. Acta 603*, 298−312.
47. Lee, K. H., Fitton, J. E., and Wuthrich, K. (1987) *Biochim. Biophys. Acta 911*, 144−153.
48. Wishart, D. S., Sykes, B. D., and Richards, F. M. (1992) *Biochemistry 31*, 1647−1651.
49. Pellegrini, M., Bisello, A., Rosenblatt, M., Chorev, M., and Mierke, D. F. (1997) *J. Med. Chem. 40*, 3025−3031.
50. Piserchio, A., Usdin, T., and Mierke, D. F. (2000) *J. Biol. Chem. 275*, 27284−27290.
51. Whitehead, T. L., McNair, S. D., Hadden, C. E., Young, J. K., and Hicks, R. P. (1998) *J. Med. Chem. 41*, 1497−1506.
52. Havel, T. F. (1990) *Biopolymers 29*, 1565−1585.
53. Lefkowitz, R. J., Cotecchia, S., Samama, P., and Costa, T. (1993) *Trends Pharmacol. Sci. 14*, 303−307.
54. Wess, J. (1997) *FASEB J. 11*, 346−354.
55. Marinissen, M. J., and Gutkind, J. S. (2001) *Trends Pharmacol. Sci. 22*, 368−376.
56. Eason, M. G., and Liggett, S. B. (1995) *J. Biol. Chem. 270*, 24753−24760.
57. Jewell-Motz, E. A., Donnelly, E. T., Eason, M. G., and Liggett, S. B. (1997) *Biochemistry 36*, 8858−8863.
58. Higashijima, T., Burnier, J., and Ross, E. M. (1990) *J. Biol. Chem. 265*, 14176−14186.
59. Mousli, M., Bueb, J. L., Bronner, C., Rouot, B., and Landry, Y. (1990) *Trends Pharmacol. Sci. 11*, 358−362.
60. Holler, C., Freissmuth, M., and Nanoff, C. (1999) *Cell. Mol. Life Sci. 55*, 257−270.
61. Yang, K., Farrens, D. L., Altenbach, C., Farahbakhsh, Z. T., Hubbell, W. L., and Khorana, H. G. (1996) *Biochemistry 35*, 14040−14046.
62. Altenbach, C., Yang, K., Farrens, D. L., Farahbakhsh, Z. T., Khorana, H. G., and Hubbell, W. L. (1996) *Biochemistry 35*, 12470−12478.
63. Ghanouni, P., Steenhuis, J. J., Farrens, D. L., and Kobilka, B. K. (2001) *Proc. Natl. Acad. Sci. U.S.A. 98*, 5997−6002.
64. Ghanouni, P., Gryczynski, Z., Steenhuis, J. J., Lee, T. W., Farrens, D. L., Lakowicz, J. R., and Kobilka, B. K. (2001) *J. Biol. Chem. 276*, 24433−24436.

BI0259610